City Research Online

City St George's, University of London

Citation: Tozer, G. M., Daniel, R. A., Lunt, S. J., Reyes-Aldasoro, C. C. & Cunningham, V. J. (2014). Haemodynamics and Oxygenation of the Tumor Microcirculation. In: Weigert, R. (Ed.), Advances in Intravital Microscopy. (pp. 125-141). Dordrecht, Netherlands: Springer Netherlands. ISBN 978-94-017-9360-5 doi: 10.1007/978-94-017-9361-2_6

This is the accepted version of the paper.

This version of the publication may differ from the final published version. To cite this item please consult the publisher's version.

Permanent repository link: https://openaccess.city.ac.uk/id/eprint/5485/

Link to published version: https://doi.org/10.1007/978-94-017-9361-2_6

Copyright and Reuse: Copyright and Moral Rights remain with the author(s) and/or copyright holders. Copies of full items can be used for personal research or study, educational, or not-for-profit purposes without prior permission or charge, unless otherwise indicated, provided that the authors, title and full bibliographic details are credited, a hyperlink and/or URL is given for the original metadata page and the content is not changed in any way. For full details of reuse please refer to City Research Online policy.

City Research Online: http://openaccess.city.ac.uk/ publications@citystgeorges.ac.uk

Chapter 6
Haemodynamics and Oxygenation of the Tumor Microcirculation

Gillian M Tozer[1,4], Rachel Daniel[1], Sarah Jane Lunt[1], Constantino C Reyes-Aldasoro[2] and Vincent J Cunningham[3]

[1] Tumor Microcirculation Group, CR-UK/YCR Sheffield Cancer Research Centre, The University of Sheffield, Department of Oncology, F Floor, School of Medicine, Beech Hill Road, Sheffield, S10 2RX, UK

[2] School of Engineering and Mathematical Sciences, City University London, London EC1V OHB, UK

[3]Aberdeen Biomedical Imaging Centre, Institute of Medical Sciences, University of Aberdeen, Forester Hill, Aberdeen, AB25 2ZD

[4]Author for correspondence
e-mail address: g.tozer@sheffield.ac.uk
Telephone: +44 (0)114 2712834

ABSTRACT

Abnormalities of the tumor vasculature and their consequences on the microenvironment of tumor cells impact on tumor progression and response to both blood-borne anti-cancer agents and radio-therapy, as well as making tumor blood vessels a target for therapy in their own right. Intravital microscopy of experimental tumors, most commonly grown in 'window' chambers, such as the dorsal skin fold chamber in mice and rats, enables investigations of tumor microcirculatory function. This is needed both to understand the molecular control of tumor vascular function and to measure the response of the vasculature to treatment. In particular, intravital microscopy enables parameters associated with blood supply, vascular permeability and oxygenation to be estimated, at high spatial and temporal resolution. In this chapter, methods used for measuring a range of these parameters, specific examples of their applications, the significance of findings and some of the limitations of the techniques are described.

6.1 Introduction

Intravital microscopy is one of the few research techniques available to study functional aspects of the tumor microcirculation. Reliance of tumor growth and metastasis on tumor vascular function makes the tumor vasculature a sought after therapeutic target. Furthermore, abnormalities of the tumor vasculature and their microenvironmental consequences, such as hypoxia and raised interstitial fluid pressure, also impact on tumor progression and therapeutic response to various treatment modalities. Optimum progression on exploiting these targets requires an understanding of the processes involved in tumor vascularization, the functional abnormalities of the tumor vasculature and analysis of response to therapy. A large part of what is known to date in these areas has been revealed from studies using intravital microscopy, which has been a mainstay of tumor microcirculation research since the first demonstration, in 1924, of a surgically implanted transparent 'window' chamber for studies of growing tissue (Sandison, 1924).

The dorsal skin fold chamber (DSFC), in mice or rats, is currently the most commonly used surgical preparation for studying the tumor microcirculation because it allows for both bright-field and fluorescence microscopy of developing tumor vasculature for periods up to several weeks. Its construction has changed little from the late 1970s (Papenfuss et al., 1979) and consists of a metal chamber (usually aluminium or titanium) supporting a skin flap, in which dermal layers from one or both sides of the flap are removed for optical clarity. A tumor fragment or cell suspension is implanted onto the exposed striated muscle layer (panniculus carnosus) and protected by a glass coverslip (Koehl et al., 2009). Developments of this model include the cranial chamber (Monsky et al., 2002), mammary gland chamber (Shan et

al., 2003), lung observation chamber (Hatakawa et al., 2002) and 'body wall' chamber that allow access to tissues for orthotopic tumor transplantation (Tsuzuki et al., 2001, Ritsma et al., 2013). Uses for the DSFC and other chamber techniques in the field of tumor angiogenesis and microcirculation are continuously evolving, as developments are made for both 2- and 3-dimensional imaging in fluorescent/bioluminescent probe design, microscopy, camera systems and image acquisition/analysis technology. Thus, intravital microscopy is set to continue playing an important role in this field for many years to come. Potential limitations associated with use of the DSFC are highlighted in Box 1.

BOX 1 It is important to recognize some fundamental limitations of intravital microscopy techniques for tumor studies, which are not overcome by modern technology. Specifically referring to the DSFC, tumors are essentially sub-cutaneous and tumor size is limited by the dimensions of the chamber, which exerts considerable tissue pressure. The surgery is relatively time-consuming and can induce bleeding, inflammation and growth of granulation tissue. Over-stretching of the skin and over- or under-tightening of retaining screws can cause problems and chambers may sag with time after surgery. As with other animal experiments, general anaesthesia can cause major haemodynamic changes. In order to avoid these, conscious mice can be restrained in specially designed jigs for microscopy, noting that the restraint itself will also impact on the animal's physiology. Consideration also needs to be given to temperature control, toxicity of contrast agents and photo-toxicity.

In this chapter, we discuss some of the methods used for functional studies of the tumor microcirculation that relate to *tumor blood supply*, *vascular permeability* and *oxygenation*.

6.2 Tumor blood supply

6. 2.1 Significance

The tumor blood supply plays a critical role in cancer therapy, knowledge of which is central to understanding the angiogenic process, by which most tumors vascularise. Blood flow is a major determinant of the delivery rate of oxygen and nutrients to tissue and so is intimately related to tumor growth and progression. In cancer therapy, blood flow to a tumor determines drug delivery. Tumor oxygenation levels, which are critically dependent on oxygen delivery, classically impact on radio-sensitivity and response to certain chemotherapeutic drugs. Therefore, quantitative measures of a tumor's blood supply are essential for understanding the role of the tumor microcirculation in tumor progression and treatment outcome. In addition, the tumor microcirculation is a direct target for anti-angiogenic and vascular disrupting cancer therapy, for which quantitative measures of tumor blood supply are required for relevant and sensitive pharmacodynamic end-points.

6.2.2 Functional measures of tumor blood supply

Definitions

The most definitive measure of a tissue's blood supply is *blood flow rate*. This is defined as the rate of delivery of arterial blood to the capillary beds within a particular mass of tissue. The units are mls of blood per unit mass of tissue per minute (ml.g-

^{1}.min^{-1}) or per unit volume of tissue per minute (ml.ml^{-1}.min^{-1}). Small, lipid-soluble, metabolically inert molecules, which rapidly cross the vascular wall and diffuse through the extra-vascular space, are useful as blood flow markers. In this case, the fraction of marker crossing the capillary vascular wall from the blood in a single pass through the tissue (extraction fraction, *E*) is close to 1.0 and for fully perfused tissue the accessible volume fraction (α) of the tissue is also close to 1.0. For a short period after intra-venous injection, net uptake rate of this type of marker into tissue is determined primarily by blood flow rate. Use of this type of marker has normally employed radioactive isotope labeling for ease of detection and sensitivity, which enables concentration of the marker to be used at true tracer levels. Quantitative estimation of tissue blood flow rate can be made from measurement of an arterial input function and a tissue response function (Tozer et al., 2009). If suitable radioactive isotopes such as ^{14}C or ^{125}I are used to label the tracer, high spatial resolution maps of blood flow rate can be obtained by measuring tissue radioactivity with autoradiograpy or phosphor imaging, at the end of the experiment. Similar computational methods are commonly applied in clinical positron emission tomography (PET) (Lammertsma et al., 1990) and, using markers at non-tracer concentrations, in dynamic contrast-enhanced magnetic resonance imaging (DCE-MRI) (Tofts et al., 1999). These methods are more difficult to apply to intravital microscopy, especially when using conventional 2-D fluorescence microscopy, mainly because of the difficulty in relating measured fluorescence intensity to true marker concentration (Waters, 2009). In order to investigate blood supply to tumors growing in the DSFC, two parameters that are related to blood flow rate have been measured instead, namely *red blood cell velocity* (RBC velocity) and the so-called *blood supply time* (BST). It should be noted that there is no direct relationship

between either RBC velocity or BST and blood flow rate, as defined above. This is most easily seen from the classical relationship known as the *central volume principle* (Stewart, 1894) that relates tissue blood flow rate (*F in ml.g^{-1}.min^{-1}*) to fractional blood volume of the tissue (*V in ml.g^{-1}*):

$$\tau = V/F \quad \text{Equation 1}$$

where τ is the capillary mean transit time (the average time taken for blood to pass through a particular capillary bed). From this equation, it can be seen that τ is only indirectly proportional to *F*, if *V* is constant and τ can only provide a quantitative measure of *F* if *V* can be measured simultaneously. Notwithstanding this caveat, measurements of both *RBC velocity* and *BST* have revealed important insights into the tumor microcirculation.

Red blood cell velocity (RBC velocity)

RBC velocity can be measured relatively easily by intravital microscopy using either commercially or freely available tracking algorithms (Reyes-Aldasoro et al., 2008a, Reyes-Aldasoro et al., 2011) (Figure 1). Tracking techniques require fast camera frame rates and fluorescence labeling of a fraction of circulating red blood cells, which normally entails injecting a small volume of red blood cells that have been labeled *ex vivo* with a membrane-binding dye[1] into the animal's circulation and tracking their passage through individual vessel segments over time. Alternatively, if the passage of red cells along a particular vessel segment is relatively sparse, slit devices can be used to monitor the interference pattern of light reaching the camera, caused by the traversing red cells. A fluorescent plasma marker, such as a FITC-

[1] A membrane marker commonly used is DiI (1,1'-dioctadecyl-3,3,3'3'-tetramethylindocarbocyanine perchlorate), an indocarbocyanine dye retained in lipid bi-layers.

labelled dextran is usually employed, so that red cells appear dark on a bright background. By matching the interference patterns recorded via the individual slits, which record at known distances along a vessel segment, RBC velocity can be calculated (Jain et al., 2013). This technique, known as temporal correlation velocimetry, was developed by Intaglietta and colleagues and has been used for many decades (Intaglietta and Tompkins, 1973). Similar principles have recently been applied on a pixel-by-pixel basis, where optical signals at each spatial location are compared with neighbouring locations over time, so that a series of cross-correlations are used to calculate both speed and direction of blood flow (Fontanella et al, 2013) in the form of 2-dimensional maps. When used with conventional single photon microscopy, the true *RBC velocity* is approximated by the measured *RBC velocity in the plane of the image*. Measurement of *RBC velocity* has been used primarily to monitor effects of treatment such as anti-angiogenic agents (Strieth et al., 2006), vascular disrupting agents (Tozer et al., 2001), photodynamic therapy (Schacht, Abels, 2006) and liposomes encapsulating chemotherapeutics (Chen et al., 2004, Strieth et al., 2004). In addition, *RBC velocity* has been used to monitor the process of vascular normalization (Akerman et al., 2013) that can occur after various cancer treatments, most notably following anti-angiogenic therapy, where vascular pruning and/or a reduction in vascular permeability can lead to improved tumor perfusion and delivery of low molecular weight chemotherapeutic drugs (Carmeliet and Jain, 2011).

Measurements of *RBC velocity* have also been combined with measurements of red blood cell flux (number of red blood cells traversing a vessel segment per unit time) to calculate tumor microvascular haematocrit (Brizel et al., 1993). Red cell flux is highly variable in the tumor microcirculation and intravital microscopy studies have

shown that large temporal changes in red cell flux can occur over short time-scales (tens of minutes). These acute fluctuations were shown to temporally co-ordinate with measured changes in oxygen partial pressure in the nearby tumor parenchyma, especially in poorly vascularized tumor regions, demonstrating that acute periods of severe tumor hypoxia, which could impact on tumor progression and therapy, can occur quite commonly (Kimura et al., 1996).

Measurements of *RBC velocity (RBCv)* have also been combined with morphological measurements of blood vessel segments to calculate each segment's *volume blood flow rate (F_{seg})*, assuming that the RBCs are traveling with the bulk plasma flow and using the formula:

$$F_{seg} = RBCv * \pi/4 * d^2 \quad \text{Equation 2}$$

where *d* is vessel segment diameter

This should not be confused with *blood flow rate (F)* as defined above, which refers to the delivery rate of blood per mass or volume of tissue.

RBC velocity can also be used as an approximation for *vessel wall shear rate*. This parameter is particularly important for understanding the angiogenic process, which is influenced by endothelial cell transduction of mechanical signals from flowing cells across their lumenal surface (Egginton, 2011).

Recently, a method for estimating *RBC velocity* and related parameters in 3-dimensional intravital images, utilizing multi-photon fluorescence microscopy (MPFM) imaging, has been developed (Kamoun et al., 2010). This method involves a fluorescent plasma marker, as above, and scanning the central axes of blood vessels at

high frequency. The angle of the resulting streaked signals in the space-time plot provides a measure of RBC velocity.

Blood supply time (BST)

The blood supply time (BST), although related to RBC velocity, is calculated from the dynamics of plasma, rather than red blood cell, flow. Developed by Rofstad and colleagues (Øye et al., 2008), intravital microscopy is used to rapidly image the first-pass of a high molecular weight contrast agent (e.g. 155 kDa TRITC-dextran) through the tumor microcirculation, following intravenous injection. Typical images used for this type of analysis are shown in Figure 2. BST is defined, for each pixel within the vascular image, as the time difference between the frame showing maximum fluorescence intensity in the pixel and the frame showing maximum fluorescence intensity in the tumor-supplying artery. This enables pixel-by-pixel maps of BST to be constructed for regional analysis of spatial blood flow heterogeneity. Repetition of this process over 20 minute time intervals within the same tumors also demonstrated substantial temporal heterogeneity in BST in A-07 human melanoma tumors (Brurberg et al., 2008). The same group has used this technique to investigate the effects of chronic cycling hypoxia (Gaustad et al., 2013), differing angiogenesis-related gene profiles (Simonsen et al., 2013) and anti-angiogenic treatment (Gaustad et al., 2012) on blood flow in xenografted human melanomas.

6.3 Tumor vascular permeability

6.3.1 Significance

The tumor blood vessel wall constitutes an obvious barrier between tumor tissue and blood-borne anti-cancer agents and controls protein transport between blood and tissue. However, high vascular permeability to macromolecules is a characteristic feature of the tumor vasculature, with established links to tumor angiogenesis, progression and poor treatment outcome (McDonald and Baluk, 2002, Lunt et al., 2009). Changes in barrier function may provide an early pharmacodynamic end-point for treatment with anti-angiogenic or vascular disrupting drugs (Tozer et al., 2005). Therefore, methods for estimating tumor vascular permeability parameters are of great interest.

6.3.2 Estimation of vascular permeability

Definitions

Vascular permeability of tumor blood vessels can be studied using intravital microscopy. Typically, this involves monitoring the clearance kinetics of a fluorescently labeled molecule (usually an albumin or dextran) from the blood vessels to the interstitium, following intra-venous injection. However, a simple qualitative assessment of leakage rate, as is commonly carried out, can be misleading because of the influence of blood flow rate on the time-course of the fluorescence concentration in the capillary (C_{vess}) and hence the amount of leakage. The high spatial resolution of intravital microscopy is a major advantage over other imaging methods, allowing a direct estimation of the vascular permeability-surface area product (*PS-product*) in ml plasma per unit mass or volume of tissue per min ($ml.g^{-1}.min^{-1}$ or $ml.ml^{-1}.min^{-1}$), where P is permeability and S is the vascular surface area per volume of tissue.

Application in intravital microscopy

Analysis of intravital microscopy data can conveniently be carried out using a so-called 'Patlak plot' (Patlak et al., 1983) to obtain the *PS-product.* Here, the time-course of the ratio of the extra-vascular tissue image intensity to C_{vess} (C_t/C_{vess}) is plotted against the time-course of the ratio $\int C_{vess} / C_{vess}$, such that the curve produced tends to linearity, as it would have done had C_{vess} been constant over the whole time-course of the measurements. The slope of the line provides an estimate of *PS-product*, as illustrated in Figure 3. Furthermore, intravital microscopy provides images of vascular and tumor morphology that can be used to estimate *S*, from which *P* can be readily calculated (Reyes-Aldasoro et al., 2008b).

It is only correct to use the Patlak plot when extravasation is effectively irreversible (uni-directional) over the time-course of the experiment but this condition is usually met by using a high molecular weight contrast agent, for which *P* is relatively low. Estimation of *PS-product* using intravital microscopy *does* suffer from the same difficulties associated with obtaining accurate quantification of fluorescence intensity, as mentioned for blood flow rate, *F*, above (Yuan et al., 1993). 3D imaging of fluorescence, especially using multi-photon fluorescence techniques, have alleviated some of these problems (Reyes-Aldasoro et al., 2008b). Studies of tumor vascular permeability using this and other analytical methods within intravital microscopy have revealed specific features of the tumor vasculature. Early studies established that tumor vascular permeability is elevated compared with most normal tissues (Gerlowski and Jain, 1986), although there is an inherent variability between different tumor models (Yuan et al., 1994). Use of different molecular size markers, allowed estimation of pore sizes in the tumor vascular wall (Hobbs et al., 1998). The effect of a blocking antibody against vascular endothelial growth factor (VEGF) on vascular

permeability to albumin was investigated in tumors growing in both cranial windows and the DSFC (Yuan et al., 1996) and a high molecular weight fluorescent dextran was used to establish that the vascular disrupting agent, combretastatin A4 phosphate (CA4P), rapidly compromised the barrier function of micro-vessels in a rat sarcoma model (Figure 3 and Reyes-Aldasoro et al., 2008b).

6.4 Tumor oxygenation

6.4.1 Significance

Hypoxia was definitively recognized as a common feature of human tumors in the 1990s, although its existence had been predicted several decades earlier (Thomlinson and Gray, 1955). The ability of oxygen to radiosensitise cells was also discovered at this time (Alper and Howard-Flanders, 1956), leading to a major interest in hypoxia and its influence on tumor progression and treatment outcome, which continues to this day. Research effort into developing methods to overcome hypoxia in tumors for therapeutic benefit has gradually evolved into one where the major focus is on targeting specific points in the oxygen-sensing pathway, many of which involve the hypoxia inducible transcription factors, HIF-1 and 2 (Semenza, 2012). HIF-1, in particular, is known to induce transcription of an expanding cohort of genes (> 70) in response to hypoxia, via binding to hypoxia response elements (HREs) in the promoter regions of the genes. The hypoxia-responsive genes, such as the genes for vascular endothelial growth factor (VEGF) and glucose transporter 1 (GLUT1), are generally associated with tumor progression. Despite stimulation of angiogenesis in response to hypoxia, the neo-vasculature fails to overcome this condition and regions

of both chronic (diffusion-limited) and acute (perfusion-limited) hypoxia persist. Indeed, as tumors grow they tend to become more hypoxic. There is considerable interest in understanding more about the hypoxic condition in tumors, in order to optimize therapeutic approaches.

6.4.2 Functional measures of tumor oxygenation

Definitions

At normal hemoglobin concentrations (150 g per l blood) and under normal conditions, the oxygen concentration in blood is approximately 9 mM. Tissue oxygen concentration is dependent on the balance between oxygen consumption and delivery. Oxygen delivery (concentration per unit time) depends on blood flow rate, hemoglobin concentration in RBCs, hemoglobin oxygen saturation (sO_2), haematocrit, distance from the nearest capillaries and the oxygen diffusion coefficient in tissue. The oxygen partial pressure (pO_2) in arterial blood is approximately 13 kPa (99 mm Hg). The oxygen partial pressure (pO_2) in mixed venous blood is approximately 5 kPa (38 mm Hg). Cells become significantly radioresistant when oxygen levels drop below approximately 0.5 kPa (4 mmHg). HIF-1-alpha (HIF-1-α) is activated when oxygen levels drop below approximately 1.0 kPa (8 mmHg).

Hemoglobin oxygen saturation

Oxy- and deoxy-hemoglobin absorb light differently across the visible and near-infra-red spectrum, such that spectra obtained from intravital microscopy of tissue microvessels can be deconstructed to estimate the oxygen saturation of hemoglobin (sO_2) at distinct spatial locations within the vasculature (Shonat et al., 1997, Nighswander-Rempel et al., 2002) (Gillies et al., 2003). The availability of

sophisticated optical filtering systems, such as acousto-optic or liquid crystal tunable filters, has significantly advanced this method, known as hyperspectral imaging. Both visual and near-infra-red light can be used in either absorbance or reflection mode. Hyperspectral intravital imaging has been pioneered for tumor biology by Sorg, Dewhirst and colleagues, initially to investigate the spatial relationship between microvascular sO_2 and tumor response to hypoxia, using tumor cells engineered to express green fluorescent protein (GFP) under the control of a HRE (Sorg et al., 2005). Other basic studies have investigated the relationship between fluctuations in tumor micro-vascular oxygenation and the location of arterio-venous shunts (Sorg et al., 2008), macrophage infiltration (Choe et al., 2010) and blood flow using the BST method described above (Lee et al., 2013). Studies of therapy have demonstrated reoxygenation of tumors following radiation treatment, which correlated with an increase in glycolysis (Zhong et al., 2013) and hypoxia-induction followed by re-oxygenation induced by the vascular disrupting agent, Oxi4503 (Wankhede et al., 2010). Examples of tumor microvascular sO_2 values from Lee et al., 2013, are shown in Figure 4.

Phosphorescence life-time imaging

The phosphorescence induced by light excitation of porphyrin derivatives is rapidly quenched by oxygen, providing a method for estimating pO_2 in tumors. Helmlinger *et al.* (Helmlinger et al., 1997) applied this technique to intravital microscopy of LS174T human colon adenocarcinoma xenografts and compared measurements with regional measurements of *pH*, using the pH-sensitive fluorochrome 2', 7' –bis-(2-carboxyethyl)-5,6-carboxyfluorescein (BCECF). Phosphorescence life-time imaging provided pO_2 measurements in intra- and extra-vascular tumor regions at 10 μm

spatial resolution. They found a complex relationship between *pH* and pO_2 at a local level, although there was a strong correlation between mean *pH* and pO_2 profiles. pO_2 gradients away from blood vessels were highly variable but consistently low in avascular areas and at distances greater than 150 μm from the supporting vasculature. Phosphorescence life-time imaging of a porphyrin derivative confined to the tumor vasculature also revealed the existence of longitudinal vascular gradients of pO_2 from the arterial to the venous side of the tumor microcirculation, in the rat mammary adenocarcinoma (R3230AC) model (Dewhirst et al., 1999). This study neatly exploited two different excitation wavelengths to excite the porphyrin through different tissue depths away from the tumor-supplying arterioles in the fascial plane (approximately 50 and 200 μm for blue and green light respectively). Oxyphor G2 was used in a subsequent study to compare oxygenation levels in three murine tumor models; K1735 malignant melanoma, RENCA renal cell carcinoma and Lewis lung carcinoma (Ziemer et al., 2005). The different patterns of oxygenation across the tumor types correlated well with the spatial distributions of oxygenation revealed by the oxygen-sensitive tissue binding of the nitroimidazole, EF5.

Other phosphorescent markers have been developed more recently for *in vivo* application. A polymer-based nano-particle with both fluorescence and phosphorescence properties enabled a technique to be used for measuring the ratio of oxygen-sensitive phosphorescence against a fluorescence standard, thus negating the need for specialized equipment for phosphorescence life-time imaging (Palmer et al., 2010). In this case, the nano-particle solution was suffused over the surface of the tumor, beneath the cover-slip of the DSFC, to provide an oxygen-sensitive overlay. The tissue pO_2 values obtained were found to correlate significantly with estimates of

hemoglobin oxygen saturation, using the hyperspectral imaging technique described above, and to associate with HIF-1 activity assayed using a GFP-based reporter system. Other developments include a platinum(II)-octaethyl-porphyrin in a transparent thin film format. This has been tested in a hamster model, using the amelanotic melanoma A-Mel-3 growing in the DSFC (Babilas et al., 2005). The thin film was applied directly to the coverslip, so that it was in contact with both tumor and surrounding normal tissue and could be excited by a LED array. Following suitable calibration, tumor pO_2 values were recorded, which were in good agreement with previous surface oxygen electrode measurements.

6.5 Concluding remarks

Intravital microscopy has played, and continues to play, a vital role in studies designed to develop an understanding of the functional aspects of the tumor microcirculation and its response to therapy. It is still a challenge to obtain fully quantifiable data on vascular function routinely and with sufficient spatial and numerical accuracy to allow detection of subtle changes with therapy. However, innovative technical developments continue apace and developments in micro-endoscopy, for instance, hold the promise of translating quantitative intravital microscopy studies of tumor vascular function to deep-seated human tumors for therapeutic benefit. Simultaneous application of intravital microscopy with other imaging modalities in clinical use, such as MRI and PET, provides an opportunity to maximise the advantages and overcome the disadvantages of each modality.

Acknowledgements

The authors' research was funded by a Programme Grant from Cancer Research UK.

REFERENCES

AKERMAN, S., FISHER, M., DANIEL, R. A., LEFLEY, D., REYES-ALDASORO, C. C., LUNT, S. J., HARRIS, S., BJORNDAHL, M., WILLIAMS, L. J., EVANS, H., BARBER, P. R., PRISE, V. E., VOJNOVIC, B., KANTHOU, C. & TOZER, G. M. 2013. Influence of soluble or matrix-bound isoforms of vascular endothelial growth factor-A on tumor response to vascular-targeted strategies. Int J Cancer. Dec 1;133(11):2563-76. doi: 10.1002/ijc.28281. Epub 2013 Jul 10.

ALPER, T. & HOWARD-FLANDERS, P. 1956. Role of oxygen in modifying the radiosensitivity of E. coli B. Nature, 178**,** 978-9.

BABILAS, P., LIEBSCH, G., SCHACHT, V., KLIMANT, I., WOLFBEIS, O. S., SZEIMIES, R. M. & ABELS, C. 2005. In vivo phosphorescence imaging of pO2 using planar oxygen sensors. Microcirculation, 12**,** 477-87.

BRIZEL, D. M., KLITZMAN, B., COOK, J. M., EDWARDS, J., ROSNER, G. & DEWHIRST, M. W. 1993. A comparison of tumor and normal tissue microvascular hematocrits and red cell fluxes in a rat window chamber model. Int. J. Radiat. Oncol. Biol. Phys., 25**,** 269-276.

BRURBERG, K. G., GAUSTAD, J. V., MOLLATT, C. S. & ROFSTAD, E. K. 2008. Temporal heterogeneity in blood supply in human tumor xenografts. Neoplasia, 10**,** 727-35.

CARMELIET, P. & JAIN, R. K. 2011. Principles and mechanisms of vessel normalization for cancer and other angiogenic diseases. Nat Rev Drug Discov, 10**,** 417-27.

CHEN, Q., TONG, S., DEWHIRST, M. W. & YUAN, F. 2004. Targeting tumor microvessels using doxorubicin encapsulated in a novel thermosensitive liposome. Mol. Cancer Ther., 3**,** 1311-7.

CHOE, S. W., ACHARYA, A. P., KESELOWSKY, B. G. & SORG, B. S. 2010. Intravital microscopy imaging of macrophage localization to immunogenic particles and co-localized tissue oxygen saturation. Acta Biomat., 6**,** 3491-8.

DEWHIRST, M., ONG, E., BRAUN, R., SMITH, B., KLITZMAN, B., EVANS, S. & WILSON, D. 1999. Quantification of Longitudinal Tissue p O_2 Gradients in Window Chamber Tumors: Impact on Tumor Hypoxia. Br. J. Cancer., 79**,** 1717-1722.

EGGINTON, S. 2011. In vivo shear stress response. Biochem. Soc. Trans., 39**,** 1633-8.

GAUSTAD, J. V., SIMONSEN, T. G., LEINAAS, M. N. & ROFSTAD, E. K. 2012. Sunitinib treatment does not improve blood supply but induces hypoxia in human melanoma xenografts. BMC cancer, 12**,** 388.

GAUSTAD, J. V., SIMONSEN, T. G., ROA, A. M. & ROFSTAD, E. K. 2013. Tumors exposed to acute cyclic hypoxia show increased vessel density and delayed blood supply. Microvasc. Res., 85**,** 10-5.

GERLOWSKI, L. E. & JAIN, R. K. 1986. Microvascular permeability of normal and neoplastic tissues. Microvasc. Res., 31**,** 288-305.

GILLIES, R., FREEMAN, J. E., CANCIO, L. C., BRAND, D., HOPMEIER, M. & MANSFIELD, J. R. 2003. Systemic effects of shock and resuscitation monitored by visible hyperspectral imaging. Diabetes Tech. Therapeut., 5**,** 847-55.

HATAKAWA, H., FUNAKOSHI, N., ONIZUKA, M., YANAGI, K., OHSHIMA, N., SATOH, Y., YAMAMOTO, T. & ISHIKAWA, S. 2002. Blood flow does not correlate with the size of metastasis in our new intravital observation model of Lewis lung cancer. Microvasc. Res., 64**,** 32-7.

HELMLINGER, G., YUAN, F., DELLIAN, M. & JAIN, R. K. 1997. Interstitial pH and pO_2 gradients in solid tumors in vivo: high-resolution measurements reveal a lack of correlation. Nature Med., 3**,** 177-182.

HOBBS, S. K., MONSKY, W. L., YUAN, F., ROBERTS, W. G., GRIFFITH, L., TORCHILIN, V. P. & JAIN, R. K. 1998. Regulation of transport pathways in tumor vessels: role of tumor type and microenvironment. Proc. Nat. Acad. Sci. USA, 95**,** 4607-12.

INTAGLIETTA, M. & TOMPKINS, W. R. 1973. Microvascular measurements by video image shearing and splitting. Microvasc. Res., 5**,** 309-12.

JAIN, R. K., MUNN, L. L. & FUKUMURA, D. 2013. Measuring angiogenesis and hemodynamics in mice. Cold Spring Harbor Protocols, 2013**,** 354-8.

KAMOUN, W. S., CHAE, S. S., LACORRE, D. A., TYRRELL, J. A., MITRE, M., GILLISSEN, M. A., FUKUMURA, D., JAIN, R. K. & MUNN, L. L. 2010. Simultaneous measurement of RBC velocity, flux, hematocrit and shear rate in vascular networks. Nature Methods, 7**,** 655-60.

KIMURA, K., BRAUN, R. D., ONG, E. T., HSU, R., SECOMB, T. W., PAPAHADJOPOULOS, D., HONG, K. & DEWHIRST, M. W. 1996. Fluctuations in red cell flux in tumor microvessels can lead to transient hypoxia and reoxygenation in tumor parenchyma. Cancer Res., 56**,** 5522-5528.

KOEHL, G. E., GAUMANN, A. & GEISSLER, E. K. 2009. Intravital microscopy of tumor angiogenesis and regression in the dorsal skin fold chamber: mechanistic insights and preclinical testing of therapeutic strategies. Clin Exp Metastasis, 26**,** 329-44.

LAMMERTSMA, A. A., CUNNINGHAM, V. J., DEIBER, M. P., HEATHER, J. D., BLOOMFIELD, P., NUTT, J., FRACKOWIAK, R. S. J. & JONES, T. 1990. Combination of dynamic and integral methods for generating reproducible functional CBF images. J. Cereb. Blood Flow Metab., 10**,** 675-686.

LEE, J. A., KOZIKOWSKI, R. T. & SORG, B. S. 2013. Combination of spectral and fluorescence imaging microscopy for wide-field in vivo analysis of microvessel blood supply and oxygenation. Optics Letters, 38**,** 332-4.

LUNT, S. J., CHAUDARY, N. & HILL, R. P. 2009. The tumor microenvironment and metastatic disease. Clin. Exp. Metastasis, 26**,** 19-34.

MCDONALD, D. M. & BALUK, P. 2002. Significance of blood vessel leakiness in cancer. Cancer Res., 62**,** 5381-5.

MONSKY, W. L., MOUTA CARREIRA, C., TSUZUKI, Y., GOHONGI, T., FUKUMURA, D. & JAIN, R. K. 2002. Role of host microenvironment in angiogenesis and microvascular functions in human breast cancer xenografts: mammary fat pad versus cranial tumors. Clin. Cancer Res., 8**,** 1008-13.

NIGHSWANDER-REMPEL, S. P., ANTHONY SHAW, R., MANSFIELD, J. R., HEWKO, M., KUPRIYANOV, V. V. & MANTSCH, H. H. 2002. Regional variations in myocardial tissue oxygenation mapped by near-infrared spectroscopic imaging. J Mol Cell. Cardiol., 34**,** 1195-203.

ØYE, K. S., GULATI, G., GRAFF, B. A., GAUSTAD, J. V., BRURBERG, K. G. & ROFSTAD, E. K. 2008. A novel method for mapping the heterogeneity in blood supply to normal and malignant tissues in the mouse dorsal window chamber. Microvasc. Res., 75**,** 179-87.

PALMER, G. M., FONTANELLA, A. N., ZHANG, G., HANNA, G., FRASER, C. L. & DEWHIRST, M. W. 2010. Optical imaging of tumor hypoxia dynamics. J. Biom. Optics, 15**,** 066021.

PAPENFUSS, H. D., GROSS, J. F., INTAGLIETTA, M. & TREESE, F. A. 1979. A transparent access chamber for the rat dorsal skin fold. Microvasc. Res., 18**,** 311-318.

PATLAK, C. S., BLASBERG, R. G. & FENSTERMACHER, J. D. 1983. Graphical evaluation of blood-to-brain transfer constants from multiple-time uptake data. J. Cereb. Blood Flow Metab., 3**,** 1-7.

REYES-ALDASORO, C. C., AKERMAN, S. & TOZER, G. M. 2008a. Measuring the velocity of fluorescently labelled red blood cells with a keyhole tracking algorithm. J. Microsc., 229**,** 162-73.

REYES-ALDASORO, C. C., GRIFFITHS, M. K., SAVAS, D. & TOZER, G. M. 2011. CAIMAN: an online algorithm repository for Cancer Image Analysis. Comp. Meth. Prog. Biomed., 103**,** 97-103.

REYES-ALDASORO, C. C., WILSON, I., PRISE, V. E., BARBER, P. R., AMEER-BEG, S. M., VOJNOVIC, B., CUNNINGHAM, V. J. & TOZER, G. M. 2008b. Estimation of Apparent Tumor Vascular Permeability from Multiphoton Fluorescence Microscopic Images of P22 Rat Sarcomas In Vivo. Microcirculation, 15**,** 65-79.

RITSMA, L., STELLER, E. J., ELLENBROEK, S. I., KRANENBURG, O., BOREL RINKES, I. H. & VAN RHEENEN, J. 2013. Surgical implantation of an abdominal imaging window for intravital microscopy. Nature Protocols, 8**,** 583-94.

SANDISON, J. C. 1924. A new method for the microscopic study of living growing tissues by the introduction of a transparent chamber in the rabbit's ear. Anat. Rec., 28**,** 281-287.

SEMENZA, G. L. 2012. Hypoxia-inducible factors: mediators of cancer progression and targets for cancer therapy. Trends Pharmacol. Sciences, 33**,** 207-14.

SHAN, S., SORG, B. & DEWHIRST, M. W. 2003. A novel rodent mammary window of orthotopic breast cancer for intravital microscopy. Microvasc Res, 65**,** 109-17.

SHONAT, R. D., WACHMAN, E. S., NIU, W., KORETSKY, A. P. & FARKAS, D. L. 1997. Near-simultaneous hemoglobin saturation and oxygen tension maps in mouse brain using an AOTF microscope. Biophys. J., 73**,** 1223-31.

SIMONSEN, T. G., GAUSTAD, J. V., LEINAAS, M. N. & ROFSTAD, E. K. 2013. Tumor-line specific causes of intertumor heterogeneity in blood supply in human melanoma xenografts. Microvasc. Res., 85**,** 16-23.

SORG, B. S., HARDEE, M. E., AGARWAL, N., MOELLER, B. J. & DEWHIRST, M. W. 2008. Spectral imaging facilitates visualization and measurements of unstable and abnormal microvascular oxygen transport in tumors. J. Biomed. Opt., 13**,** 014026.

SORG, B. S., MOELLER, B. J., DONOVAN, O., CAO, Y. & DEWHIRST, M. W. 2005. Hyperspectral imaging of hemoglobin saturation in tumor microvasculature and tumor hypoxia development. J. Biomed. Opt., 10**,** 44004.

STEWART, G. N. 1894. Researches on the circulation time in organs and on the influences which affect it. J Physiol (London), 15**,** Parts I-III.

STRIETH, S., EICHHORN, M. E., SAUER, B., SCHULZE, B., TEIFEL, M., MICHAELIS, U. & DELLIAN, M. 2004. Neovascular targeting chemotherapy: encapsulation of paclitaxel in cationic liposomes impairs functional tumor microvasculature. Int. J. Cancer, 110**,** 117-24.

STRIETH, S., EICHHORN, M. E., SUTTER, A., JONCZYK, A., BERGHAUS, A. & DELLIAN, M. 2006. Antiangiogenic combination tumor therapy blocking alpha(v)-integrins and VEGF-receptor-2 increases therapeutic effects in vivo. Int. J. Cancer, 119**,** 423-31.

THOMLINSON, R. H. & GRAY, L. H. 1955. The histological structure of some human lung cancers and the possible implications for radiotherapy. Br. J. Cancer, 9**,** 539-549.

TOFTS, P. S., BRIX, G., BUCKLEY, D. L., EVELHOCH, J. L., HENDERSON, E., KNOPP, M. V., LARSSON, H. B., LEE, T. Y., MAYR, N. A., PARKER, G. J., PORT, R. E., TAYLOR, J. & WEISSKOFF, R. M. 1999. Estimating kinetic parameters from dynamic contrast-enhanced T(1)- weighted MRI of a diffusable tracer: standardized quantities and symbols. J Magn Reson Imaging, 10**,** 223-32.

TOZER, G. M., KANTHOU, C. & BAGULEY, B. C. 2005. Disrupting tumor blood vessels. Nat. Rev. Cancer, 5**,** 423-35.

TOZER, G. M., PRISE, V. E. & CUNNINGHAM, V. J. 2009. Quantitative estimation of tissue blood flow rate. Methods Mol Biol, 467**,** 271-86.

TOZER, G. M., PRISE, V. E., WILSON, J., CEMAZAR, M., SHAN, S., DEWHIRST, M. W., BARBER, P. R., VOJNOVIC, B. & CHAPLIN, D. J. 2001. Mechanisms associated with tumor vascular shut-down induced by combretastatin A-4 phosphate: intravital microscopy and measurement of vascular permeability. Cancer Res, 61**,** 6413-6422.

TSUZUKI, Y., MOUTA CARREIRA, C., BOCKHORN, M., XU, L., JAIN, R. K. & FUKUMURA, D. 2001. Pancreas microenvironment promotes VEGF expression and tumor growth: novel window models for pancreatic tumor angiogenesis and microcirculation. Lab. Invest., 81**,** 1439-51.

WANKHEDE, M., DEDEUGD, C., SIEMANN, D. W. & SORG, B. S. 2010. In vivo functional differences in microvascular response of 4T1 and Caki-1 tumors after treatment with OXi4503. Oncol. Rep., 23**,** 685-92.

WATERS, J. C. 2009. Accuracy and precision in quantitative fluorescence microscopy. J. Cell Biol., 185**,** 1135-48.

YUAN, F., CHEN, Y., DELLIAN, M., SAFABAKHSH, N., FERRARA, N. & JAIN, R. K. 1996. Time-dependent vascular regression and permeability changes in

established human tumor xenografts induced by an anti-vascular endothelial growth factor/vascular permeability factor antibody. Proc Natl Acad Sci USA, 93**,** 14765-70.

YUAN, F., LEUNIG, M., BERK, D. A. & JAIN, R. K. 1993. Microvascular permeability of albumin, vascular surface area, and vascular volume measured in human adenocarcinoma LS174T using dorsal chamber in SCID mice. Microvasc Res, 45**,** 269-89.

YUAN, F., SALEHI, H. A., BOUCHER, Y., VASTHARE, U. S., TUMA, R. F. & JAIN, R. K. 1994. Vascular permeability and microcirculation of gliomas and mammary carcinomas transplanted in rat and mouse cranial windows. Cancer Res., 54**,** 4564-4568.

ZHONG, J., RAJARAM, N., BRIZEL, D. M., FREES, A. E., RAMANUJAM, N., BATINIC-HABERLE, I. & DEWHIRST, M. W. 2013. Radiation induces aerobic glycolysis through reactive oxygen species. Radiother. Oncol., 106**,** 390-6.

ZIEMER, L. S., LEE, W. M., VINOGRADOV, S. A., SEHGAL, C. & WILSON, D. F. 2005. Oxygen distribution in murine tumors: characterization using oxygen-dependent quenching of phosphorescence. J. Appl. Physiol., 98**,** 1503-10.

FIGURES

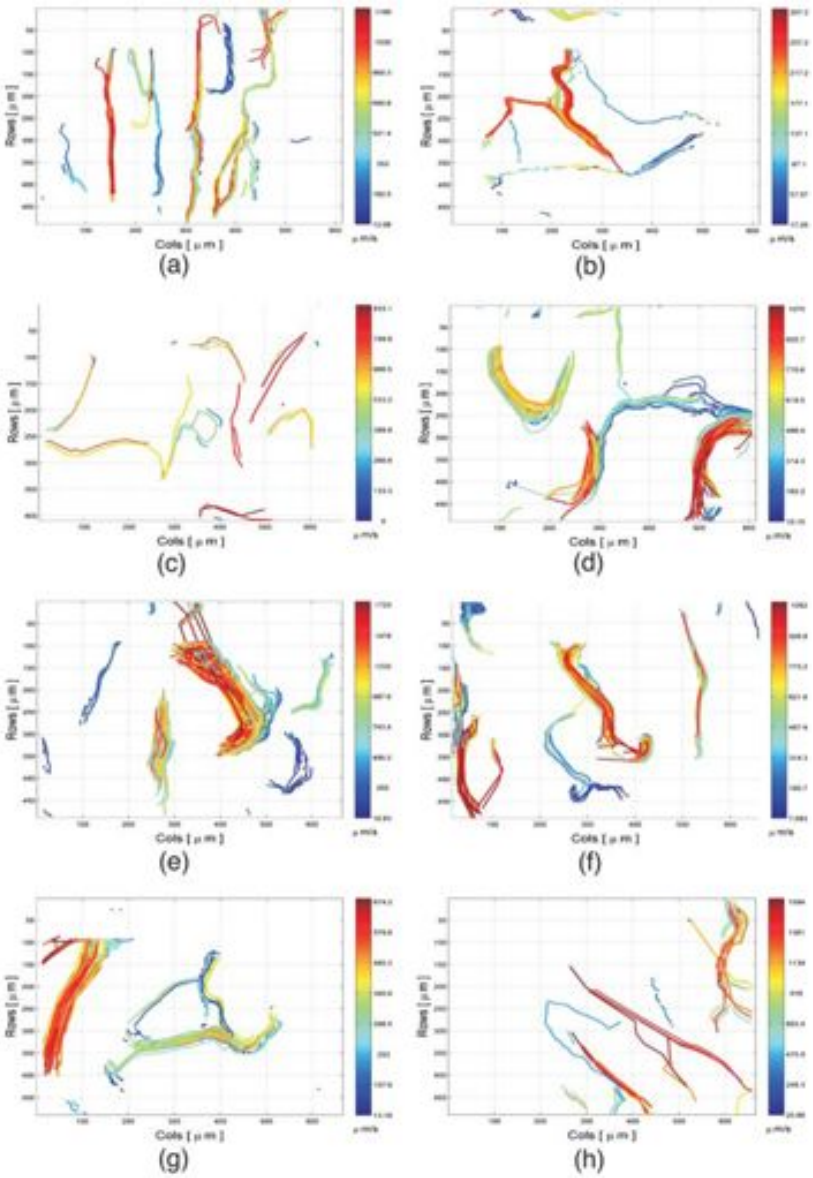

Figure 1

Examples of tracks made by red blood cells (RBC) as they flow through the tumor microcirculation. Tracks were obtained from eight different mouse fibosarcomas, a) to h). Each RBC track is represented by a line, where the direction and colour represent RBC velocity. This figure is reproduced, with permission, from Reyes-Aldasoro et al., Journal of Microscopy, 229:163-173, 2008.

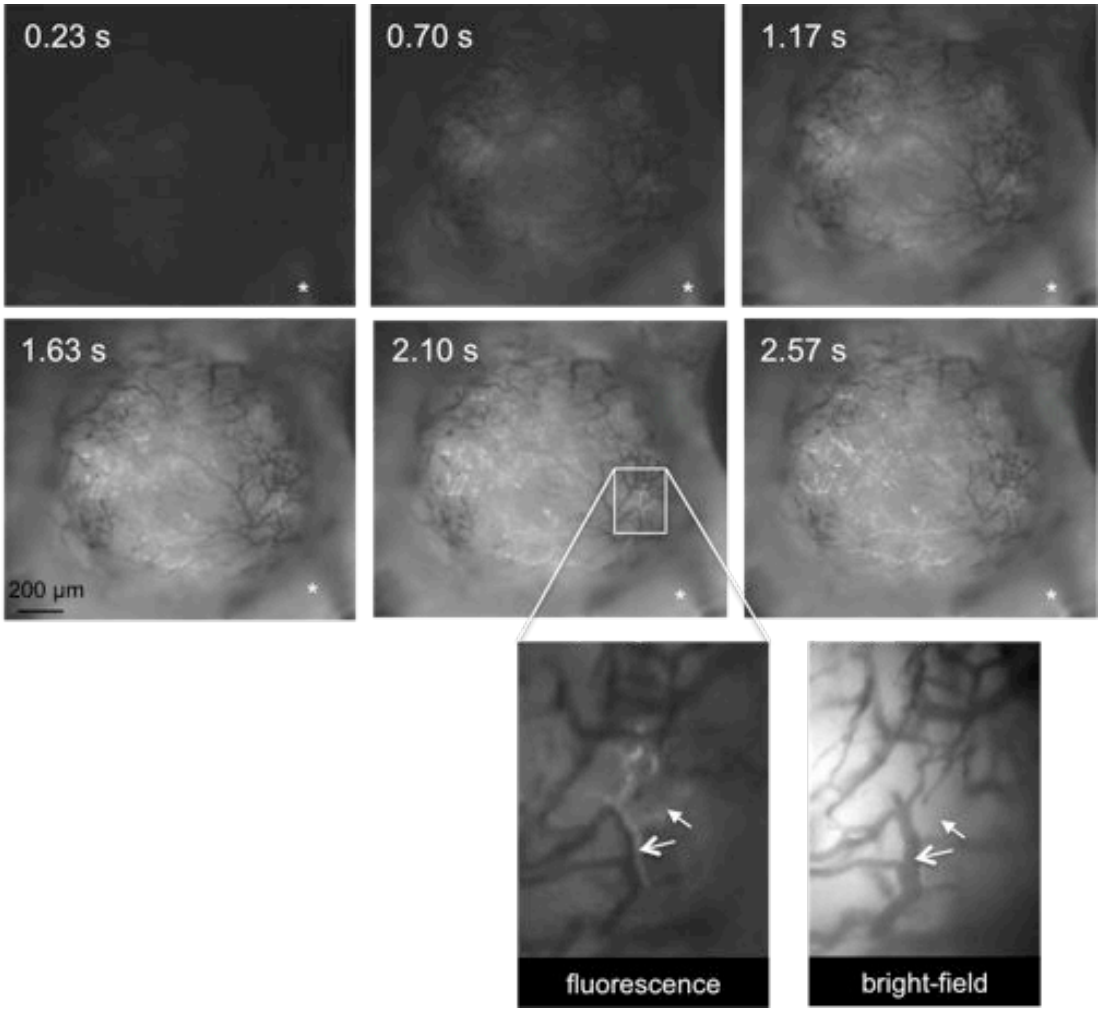

Figure 2

Top panels show a time-series of epi-fluorescence images taken of a mouse fibrosarcoma (fs188) growing in a mouse DSFC, following the intravenous injection of 80 mg/kg FITC-dextran. Times shown are relative to the appearance above background of fluorescence in a tumor supplying arteriole, indicated by * in each image. Similar images have been used to estimate the blood supply time (BST) – see main text for details. An expanded epifluorescence image and the corresponding transmitted light image are shown in the lower panels. The arrows in the epifluorescence image indicate vessel segments that have filled very rapidly with FITC-dextran, indicating that they are close to the arterial side of the micro-circulatory network. The vessel segment indicated by the open arrow lies immediately adjacent to an unfilled vessel segment. It is impossible to discriminate between these two segments in the corresponding bright-field image, where the vessel pairing appears as a single vessel (open arrow). The closed arrow indicates a rapidly filled vessel, which is hardly distinguishable in the bright-field image.

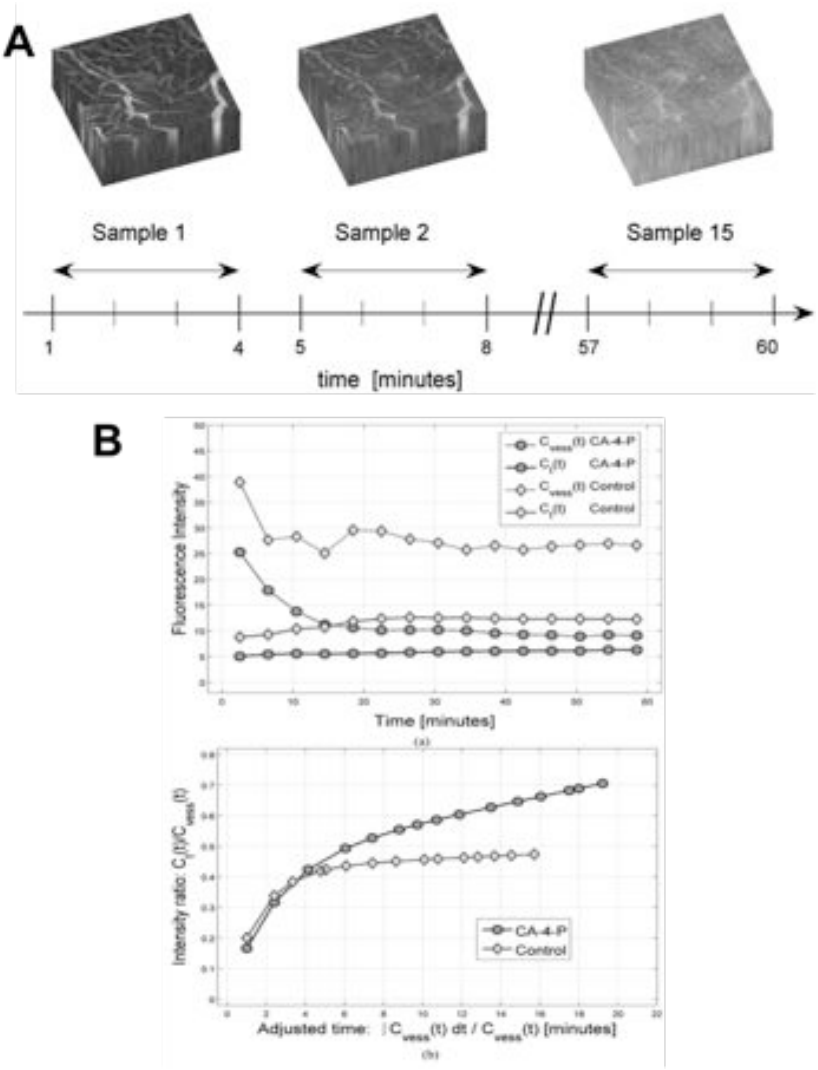

Figure 3

Panel A shows examples of a 3-D tumor volume (512 x 512 x 11 voxels corresponding to 1331.2 x 1331.2 x 50 μm^3) of fluorescence intensity images acquired using multiphoton fluorescence microscopy, at various times following intravenous injection of 40 kDa FITC-dextran to a tumor-bearing rat. A total of 15 volumes were acquired in a 60-minute time-frame, from a sub-cutaneously transplanted rat P22 sarcoma. Panel B a) shows example time-activity curves of the fluorescence intensities of intravascular tissues ($C_{vess}(t)$) and extravascular tissue ($C_t(t)$) versus time for two data sets, similar to those shown in A. Data were acquired following image segmentation into the intravascular and extravascular tissue regions. Data from one animal treated with the vascular disrupting agent, combretastatin A4 phosphate (CA-4-P), and from one control, untreated animal are shown. Panel Bb) shows the same data, as in a), transformed, as described by Patlak (Patlak et al., 1983) and in the main text. The slope of the linear portion of the curve provides the estimate of the *PS-product*. Figures A and B are reproduced, with permission, from Reyes-Aldasoro et al., Microcirculation, 15:65-79, 2008.

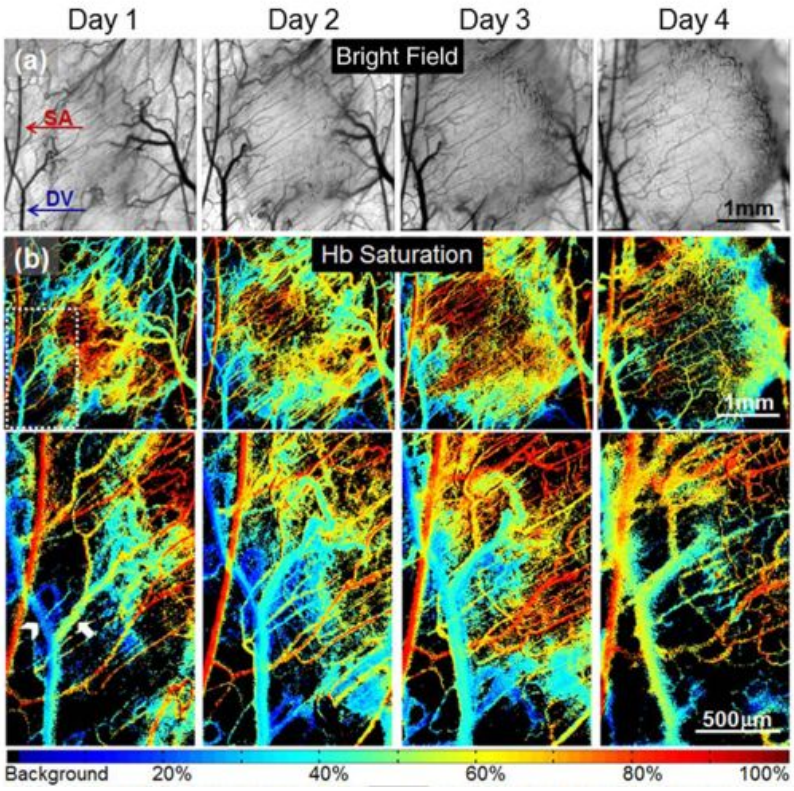

Figure 4

Examples of tumor hemoglobin oxygen saturation (sO_2) with tumor growth, estimated from hyperspectral imaging. (a) Brightfield images of the Caki-2 human renal carcinoma growing the DSFC, showing a tumor supplying artery (SA) and draining vein (DV). (b) sO2 maps corresponding to images in (a). Arrow-head indicates a venous branch from non-tumor tissue. Arrow indicates a vessel carrying shunted blood. Figure reproduced in part, with permission, from Lee et al., Optics Letters, 38:332-334, 2013.